JOURNAL OF MAGNETIC RESONANCE **134,** 17–29 (1998)
ARTICLE NO. MN981491

Efficient Simulation of Coherence Transfer Pathway Selection by Phase Cycling and Pulsed Field Gradients in NMR

Alexej Jerschow* and Norbert Müller†,[1]

*Université de Lausanne, Section de Chimie, BCH, CH-1015, Lausanne-Dorigny, Switzerland; and †Institut für Chemie, Johannes Kepler University Linz, Altenbergerstrasse 69, A-4040 Linz, Austria

Received December 23, 1997; revised April 7, 1998

DEDICATED TO PROFESSOR RICHARD R. ERNST ON THE OCCASION OF HIS 65TH BIRTHDAY

The selection of well-defined coherence transfer pathways is an essential feature of all but the simplest NMR and EPR pulse sequences. This selection can be achieved by phase cycling and by pulsed field gradients. The properties of the RF-pulses (flip angle, offset effects, inhomogeneity) and transport phenomena (diffusion, flow) in conjunction with gradients cause a weighting of the different coherence transfer pathways. We present a method by which the selection process can be simulated efficiently and visualized easily. In its basic form it involves straightforward matrix manipulations without reference to the density matrix and the particular spin system. This method is implemented in a MATLAB program, called CCCP (Complete Calculation of Coherence Pathways).

INTRODUCTION

The concepts of coherence order and coherence transfer pathways (CTPs) are important both in pulsed NMR and EPR experiments (*1–5*). The magnetization trajectories in terms of coherence orders are used to visualize the effects of pulse sequences. New pulse sequences are usually designed by designating wanted and unwanted CTPs. RF-pulses are in general nonselective with respect to the excitation or interconversion of different coherence orders, which necessitates the use of coherence pathway filtering techniques. For example, without this filtering a general three pulse NMR experiment contains simultaneously the information of MQF–COSY, NOESY, and Relayed-COSY experiments. Furthermore, no distinction between echo and anti-echo signals can be made without special coherence filtering techniques (*1–3*). Only the selection of the appropriate CTPs makes an experiment specific. Undesired CTPs give rise to spurious echoes in EPR (*4, 5*).

Phase cycling (*1, 2*) and sequences of pulsed field gradients (PFGs) (*3*) are the two most important coherence filtering techniques. Phase cycles allow the selection of parallel pathways but may take a long time, especially in sequences with many pulses, when high coherence orders and good selectivity (in terms of CTPs) are desired. Subtraction errors can become severe, especially with long intertwined phase cycles giving rise to t_1-noise in two-dimensional spectra.

Pulsed field gradients usually achieve the desired filtering in a single transient but selectivity may be limited with multiple filters, especially when only single axis gradient hardware is used (*3, 6*).

Additionally, the properties of the RF-pulses (flip angle, shape, offset effects, inhomogeneity) and translatory motion cause a weighting of the different CTPs.

A compromise between CTP selectivity and time requirement can be achieved by combining pulsed field gradients and phase cycles while reducing the number of phase steps as much as possible. Sometimes incomplete phase cycles in combination with gradients can be developed empirically, partly by trial and error. In these cases it becomes difficult to rationalize the selection process, in particular for a general spin system. It is desirable to use simulations for reasons of speed, reproducibility, and completeness with respect to the possible CTPs.

A straightforward approach would be to use an existing simulation package like, e.g., GAMMA (*7*), to calculate the evolution of the density matrix for a full phase cycle. However, this method does not yield the required information (the relative amplitudes of the different CTPs) directly. A full GAMMA simulation of all possible CTPs is not practical because of time and computer memory constraints. The number of possible CTPs in a pulse sequence is of the order $(2p_{\max} + 1)^n$ (where $p_{\max}$ is the maximum possible coherence order, and n is the number of pulses). Computer algebra approaches have been used to calculate the evolution of product operators (*8, 9*), which, however, are even less appropriate for this problem since the number of possible product operator terms rises much faster than the number of CTPs (*9*). Also, the final recombination and simplification of the algebraic expressions involves excessive use of trigonometric combination rules and is therefore very slow.

The purpose of the work presented in this article was to devise an effective scheme which can be used to simulate the CTP selection process and which involves only simple matrix calculations. Our goal was to retain as high a degree of gen-

[1] To whom correspondence should be addressed.

1090-7807/98 $25.00

erality as possible. We eventually obtained a method which can be used without reference to a particular spin system.

THEORY

Selection by Phase Cycling

Every density matrix can be expanded in a series of different components according to their behavior under rotation around the preferred z-axis (*2, 10, 11*),

$$\sigma = \sum_{p=-p_{\max}}^{p_{\max}} \sigma_p , \qquad [1]$$

where $p_{\max}$ is the maximum possible coherence order (equal to the number of spins in case of a spin $\frac{1}{2}$ only system). Upon rotation around the z-axis the σ_p acquire only a phase (*11*), since

$$\exp(i\phi F_z)\sigma_p \exp(-i\phi F_z) = \sigma_p \exp(ip\phi), \qquad [2]$$

where $F_z = \Sigma_j I_{zj}$ is the z-component of the total angular momentum.

The effect of an RF-pulse is more complicated and, in general, may cause mixing of all coherence orders. Without specifying the nature of the RF-pulse we may represent the unknown transformation by a unitary operator in the rotating frame under consideration of its relative phase ϕ:

$$U_\phi = \exp(-i\phi F_z) U \exp(i\phi F_z). \qquad [3]$$

The evolution of an initial operator σ_{p_j} during U_ϕ is then

$$\begin{aligned} U_\phi \sigma_{p_j} U_\phi^\dagger &= \exp(-i\phi F_z) U \\ &\quad \times \{\exp(i\phi F_z)\sigma_{p_j}\exp(-i\phi F_z)\} U^\dagger \exp(i\phi F_z) \\ &= \exp(-i\phi F_z) U \sigma_{p_j} \exp(ip_j\phi) U^\dagger \exp(i\phi F_z). \end{aligned} \qquad [4]$$

where use has been made of Eq. [2] to contract the terms within the braces.

To maintain generality we do not specify the operator U any further. We just state that it generates a superposition of coherences:

$$U\sigma_{p_j}U^\dagger = \sum_{p_k} c(p_j, p_k)\sigma_{p_k} \qquad [5]$$

(p_j and p_k refer to the coherence orders before and after the pulse, respectively) and we get

$$U_\phi \sigma_{p_j} U_\phi^\dagger = \exp(ip_j\phi)\exp(-i\phi F_z)\Big(\sum_{p_k} c(p_j, p_k)\sigma_{p_k}\Big)\exp(i\phi F_z). \qquad [6]$$

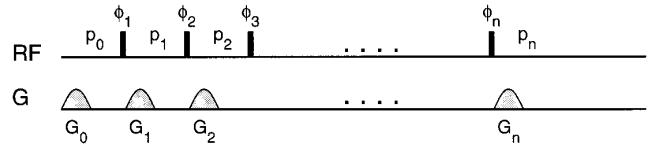

FIG. 1. Simple scheme for a general pulse sequence. n pulses separate $n + 1$ periods of free evolution during which gradient pulses G_i may be switched on with different strengths and directions. The coherence orders p_i (and the effective gyromagnetic ratios γ^*) can only change during the pulses.

Applying Eq. [2] again, we have

$$U_\phi \sigma_{p_j} U_\phi^\dagger = \sum_{p_k} c(p_j, p_k)\sigma_{p_k}\exp(-i\Delta p\phi), \qquad [7]$$

where $\Delta p = p_k - p_j$. This formula represents the well-known rule of phase cycling:

> A signal passing through a coherence transfer (by a pulse or sequence of pulses) of Δp reacts to a phase change ϕ of the pulse (or the sequence of pulses) by changing its phase by $-\Delta p\phi$.

The phase change of the signal for a pulse phase shift of $\phi = m\,2\pi/N$ (representing the mth step in an N step phase cycle) therefore is

$$\Delta\psi = -m\frac{2\pi}{N}(\Delta p + kN) = -m\frac{2\pi}{N}\Delta p - m2\pi k. \qquad [8]$$

The first term in the sum can be compensated by shifting the receiver phase to select a desired change in coherence order Δp. Coherence order changes of $\Delta p + kN$ ($k = 0, \pm1, \pm2$) will also be selected, since the second term is equal to multiples of 2π, while it is running through a complete cycle for $k = \frac{1}{N}, \frac{2}{N}, \ldots, \frac{N-1}{N}$ which leads to the cancellation of the coherence order changes in between.

The second rule follows immediately:

> Coherence order changes of $\Delta p + k \cdot N$ ($N = 2, 3, \ldots$; $k = 0, \pm1, \pm2, \ldots$) are selected by cycling the phase ϕ through N values of $m \cdot \frac{2\pi}{N}$ ($m = 0, 1, \ldots, N - 1$) and shifting the receiver phase in concert through $-m \cdot \Delta p\frac{2\pi}{N}$.

Applying the second rule for each pulse in a sequence allows one to construct complete phase cycles, which can be very large ($\Pi_j N_j$; here N_j denotes the number of phase cycling steps in the jth cycle). Such a cycle can rarely ever be used in a long pulse sequence since the duration of the experiment would increase beyond practical limits. Intuition and experience have been used to cut down the number of phase cycling steps. However, this approach is error-prone, since once the pulses are not phase shifted independently it becomes very difficult to predict which pathways are selected and to which extent they are attenuated.

For all of the following discussion we will use a schematic pulse sequence as represented in Fig. 1, which provides a very general model: A series of n RF-pulses (of any non-secular

interaction, the relative phase of which can be changed by experiment, like a pulse sandwich, or a composite pulse train) with phases ϕ_i separates $n + 1$ periods of free evolution.

Coherence orders change only during the pulses, and remain constant during free evolution. In order to maintain generality we neither restrict p_0 to zero (for the equilibrium state) nor p_n to -1 (as is the common convention for the detection coherence order). Thus we are allowed to treat parts of pulse sequences separately, to examine the appearance of quadrature images, or to investigate the CTPs of only one spin species (e.g., of ^{13}C in ^{1}H-detected experiments where $p_0 = p_n = 0$).

The coherence orders during the inter-pulse delays (evolution periods) may be cast in row vector form:

$$\mathbf{p} = (p_0, p_1, \ldots, p_n). \quad [9]$$

The pulse phases are represented by a column vector $\boldsymbol{\phi}$:

$$\boldsymbol{\phi} = (\phi_1, \phi_2, \ldots, \phi_n)^T. \quad [10]$$

Using

$$\begin{aligned}\Delta\mathbf{p} &= (\Delta p_1, \Delta p_2, \ldots, \Delta p_n)\\ &= (p_1 - p_0, p_2 - p_1, \ldots, p_n - p_{n-1})\end{aligned} \quad [11]$$

the total phase change of the coherence pathway is given according to the first rule simply by (*2, 4*)

$$\psi = -\sum_j (\Delta p_j \cdot \phi_j) - \phi_r = -\Delta\mathbf{p} \cdot \boldsymbol{\phi} - \phi_r, \quad [12]$$

where ϕ_r is the receiver phase.

For the purpose of simulation the effect of an entire phase cycle shall be cast into a matrix representation. The selection of CTPs by phase cycling is achieved by adding up the signals acquired in consecutive experiments, in which the pulse phases are changed. To describe this process we represent an entire phase cycle in matrix form,

$$\hat{\phi} = \begin{pmatrix} \phi_{11} & \phi_{12} & \cdots & \phi_{1c} \\ \phi_{21} & \phi_{22} & \cdots & \phi_{2c} \\ \cdots & \cdots & \cdots & \cdots \\ \phi_{n1} & \phi_{n1} & \cdots & \phi_{nc} \end{pmatrix}, \quad [13]$$

where n is the number of pulses and c is the number of steps of the phase cycle. The kth row of the matrix $\hat{\phi}$ represents the phase cycle for pulse k in the pulse sequence.

As a next step the matrix $\hat{p}$ of all possible CTPs is constructed,

$$\hat{p} = \begin{pmatrix} p_{10} & p_{11} & \cdots & p_{1(n-1)} & p_{1n} \\ p_{20} & p_{21} & \cdots & p_{2(n-1)} & p_{2n} \\ \cdots & \cdots & \cdots & \cdots & \cdots \\ p_{m0} & p_{m1} & \cdots & p_{m(n-1)} & p_{mn} \end{pmatrix}, \quad [14]$$

where m is the number of all possible pathways. $\Delta\hat{p}$ is given consequently by

$$\Delta\hat{p} = \begin{pmatrix} (p_{11} - p_{10}) & \cdots & (p_{1n} - p_{1(n-1)}) \\ (p_{21} - p_{20}) & \cdots & (p_{2n} - p_{2(n-1)}) \\ \cdots & \cdots & \cdots \\ (p_{m1} - p_{m0}) & \cdots & (p_{mn} - p_{m(n-1)}) \end{pmatrix}. \quad [15]$$

Using Eq. [12] we get

$$\begin{aligned}\hat{\psi} &= -\Delta\hat{p} \cdot \hat{\phi} - \hat{\phi}_r\\ &= -\begin{pmatrix} \Delta p_{11} & \cdots & \Delta p_{1n} \\ \Delta p_{21} & \cdots & \Delta p_{2n} \\ \cdots & \cdots & \cdots \\ \Delta p_{m1} & \cdots & \Delta p_{mn} \end{pmatrix} \cdot \begin{pmatrix} \phi_{11} & \phi_{12} & \cdots & \phi_{1c} \\ \phi_{21} & \phi_{22} & \cdots & \phi_{2c} \\ \cdots & \cdots & \cdots & \cdots \\ \phi_{n1} & \phi_{n1} & \cdots & \phi_{nc} \end{pmatrix}\\ &\quad - \begin{pmatrix} \phi_1^r & \phi_2^r & \cdots & \phi_c^r \\ \phi_1^r & \phi_2^r & \cdots & \phi_c^r \\ \cdots & \cdots & \cdots & \cdots \\ \phi_1^r & \phi_2^r & \cdots & \phi_c^r \end{pmatrix} = \begin{pmatrix} \psi_{11} & \psi_{12} & \cdots & \psi_{1c} \\ \psi_{21} & \psi_{22} & \cdots & \psi_{2c} \\ \cdots & \cdots & \cdots & \cdots \\ \psi_{m1} & \psi_{m2} & \cdots & \psi_{mc} \end{pmatrix},\end{aligned} \quad [16]$$

where the matrix $\hat{\phi}_r$ contains the receiver phases, which are evidently the same for all different CTPs. $\hat{\psi}$ is then a matrix whose rows represent the signal phases in each step of the phase cycle (columns) for every pathway given in $\hat{p}$ (rows).

The relative complex signal amplitude for a CTP with row index k in $\hat{p}$ is then given by

$$s_k = \sum_j \exp(-i\psi_{kj}), \quad [17]$$

which amounts to a row-wise vector summation of the phase angles ψ_{kj} in $\hat{\psi}$.

The pathways can then be sorted by their amplitude $|s_k|$, and canceled pathways may be discarded from further consideration. Thus a few simple matrix manipulations suffice to find the selected CTPs.

These results are obtained without reference to a particular spin system and are therefore universally applicable considering just the assumptions described above.

Selection by Pulsed Field Gradients

The use of PFGs in addition to phase cycling allows one to cut down the number of phase cycling steps significantly. Since attenuation of unwanted pathways occurs by averaging over the sample volume rather than over a number of transients, instrument instabilities do not cause subtraction artifacts.

Another major difference from the selection by phase cycles is that the effect of gradients depends on the coherence order p rather than on a change of coherence order Δp and also on the gyromagnetic ratio.

In the imaging literature the concept of the *effective gradient* (*12*) has been introduced to allow one to analyze pulse and

gradient sequences separately. However, this has as yet only been applied to homonuclear spin systems. In order to allow a more general treatment the *effective gyromagnetic ratio* is introduced here.

The density operator σ_p can be decomposed into

$$\sigma_p = \sum \sigma(p_1, \ldots, p_j, \ldots p_{j_{\max}}), \qquad [18]$$

where the sum runs over all combinations of p_j which satisfy $\sum_{j=1}^{j_{\max}} p_j = p$, j is the index of the nuclear species, and p_j is the (partial) coherence order of the jth nuclear species. Each of the $\sigma(p_1, \ldots, p_j, \ldots\ p_{j_{\max}})$ can be written as

$$\sigma(p_1, \ldots, p_j, \ldots p_{j_{\max}}) = \prod_j \sigma_{p_j}, \qquad [19]$$

where the product is a multiple direct product (*10*).

The gradient Hamiltonian given in units of rads per second, $H_G = \Sigma_j \gamma_j \mathbf{G}(t)\mathbf{r}I_{j,z}$ (with $\mathbf{G}(t)$ denoting the gradient strength and $\mathbf{r}$ the location in the sample, which is held constant in this case) acts separately on the subspace of the nuclear species j,

$$\sigma_{p_j} \xrightarrow{H_G} \sigma_{p_j} \exp\left[-ip_j\gamma_j\mathbf{r} \cdot \int \mathbf{G}(t)dt \right], \qquad [20]$$

which follows from Eq. [2] and the substitution $\phi = \gamma_j \mathbf{r} \cdot \int \mathbf{G}(t)dt$.

Substituting $\mathbf{h} = \int \mathbf{G}(t)dt$ and combining the transformations of all nuclear species (Eqs. [19], and [20]) we get

$$\sigma(p_1, \ldots, p_j, \ldots p_{j_{\max}}) \xrightarrow{H_G} \sigma(p_1, \ldots, p_j, \ldots p_{j_{\max}}) \exp(-i\gamma^*\mathbf{h} \cdot \mathbf{r}), \qquad [21]$$

where we have introduced the *effective gyromagnetic ratio*

$$\gamma^* = \sum_j p_j \gamma_j. \qquad [22]$$

Other secular interactions commute and may therefore be treated separately.

In the homonuclear case the effective gyromagnetic ratio has a particularly simple form:

$$\gamma^*_{\text{homo}} = p \cdot \gamma. \qquad [23]$$

The effective gradient $\mathbf{G}^*$ (*12*) is related to the effective gyromagnetic ratio through

$$\mathbf{G}^* = \frac{\gamma^*}{\gamma} \cdot \mathbf{G}. \qquad [24]$$

The relation between the effective gyromagnetic ratio and the composite coherence order p_c (which may be seen as a good quantum number under the gradient Hamiltonian) introduced in (*6*) is

$$p_c = \frac{\gamma^*}{\gamma}. \qquad [25]$$

In order to calculate the effect of an entire gradient sequence from Eq. [21] we may make use of the fact that γ^* only changes during the RF-pulses. A particular γ^* pathway can then be represented by a vector $\boldsymbol{\gamma}^* = (\gamma_0^*, \gamma_1^*, \ldots, \gamma_n^*)$. The matrix

$$\hat{h} = (h_{ij}) = \begin{pmatrix} h_{0x} & h_{1y} & h_{1z} \\ h_{1x} & h_{2y} & h_{2z} \\ \cdots & \cdots & \cdots \\ h_{nx} & h_{ny} & h_{nz} \end{pmatrix} \qquad [26]$$

contains the time integrals of the gradients in all directions in space, i.e.,

$$h_{ij} = \int_{t_i}^{t_{i+1}} G_j(t)dt, \qquad [27]$$

where t_i is the time of the ith RF-pulse ($t_0 = 0$), and $j = x, y, z$. $\hat{h}$ will be a column vector if only single axis gradients are used.

Using $\mathbf{r} = (x, y, z)^T$ the location-dependent phase acquired by a signal following a particular $\hat{\gamma}$ pathway is

$$\psi(\mathbf{r}) = \boldsymbol{\gamma}^* \cdot \hat{h} \cdot \mathbf{r} = k_x x + k_y y + k_z z, \qquad [28]$$

where $k_{x,y,z}$ represent spatial frequencies given in rads per meter (*12, 13*). In order to obtain the total signal amplitude it is necessary to calculate

$$\overline{\exp(-i\psi(\mathbf{r}))} = f_z\, f_{xy} = \overline{\exp(-i\psi(z))} \cdot \overline{\exp(-i\psi(x) - i\psi(y))}. \qquad [29]$$

The first term is evaluated in a familiar way (*2*) by

$$f_z = \overline{\exp(-i\psi(z))} = \frac{1}{2z_{\max}} \cdot \int_{-z_{\max}}^{z_{\max}} \exp(-ik_z z)dz = \operatorname{sinc}(k_z z_{\max}). \qquad [30]$$

Since the sinc function is oscillatory and can become zero, it would be possible to obtain results of the attenuation of a particular pathway that are too optimistic. To calculate the

upper limit of the attenuation, we use the envelope function of the sinc function:

$$\bar{f}_z = \begin{cases} \mathrm{sinc}(k_z z_{\max}) & \text{if } 0 \le |k_z z_{\max}| < \dfrac{\pi}{2} \\ \dfrac{1}{|k_z z_{\max}|} & \text{if } \dfrac{\pi}{2} \le |k_z z_{\max}|. \end{cases} \quad [31]$$

The calculation of the signal attenuation due to transverse gradients is somewhat more complicated in a standard NMR tube due to the circular profile over which averaging has to be performed (*13*). Although the x and y gradients are applied along orthogonal directions in space (and therefore the spatial frequencies k_x, k_y can be calculated independently) the averaging process cannot be factored into independent integrations over x and y. However, it is possible to calculate the signal attenuation by using an effective spatial frequency $k_{xy} = (k_x^2 + k_y^2)^{1/2}$ and a weighting function $(1 - (x/x_{\max})^2)^{1/2}$ to account for the circular profile

$$\begin{aligned} f_{xy} &= \overline{\exp(-i\psi(x) - i\psi(y))} \\ &= \frac{2}{\pi x_{\max}} \int_{-x_{\max}}^{x_{\max}} \left[1 - \left(\frac{x}{x_{\max}} \right)^2 \right]^{1/2} \exp(-ik_{xy}x)\,dx \\ &= \frac{2J_1(k_{xy}x_{\max})}{k_{xy}x_{\max}}, \end{aligned} \quad [32]$$

where J_k is the Bessel function of the first kind (the solution of the integral was taken from (*14*)). Again, we are rather interested in an upper bound. The relationship

$$J_1(\xi) \approx \left(\frac{2}{\pi\xi} \right)^{1/2} \cos\left(\xi - \frac{3\pi}{4} \right) \quad [33]$$

holds for large ξ (*15*), from which we deduce the envelope function

$$\bar{f}_{xy} = \begin{cases} \dfrac{2J_1(k_{xy}x_{\max})}{k_{xy}x_{\max}} & \text{if } 0 \le |k_{xy}x_{\max}| < 2.44 \\ \pi^{-1/2} \left(\dfrac{2}{k_{xy}x_{\max}} \right)^{3/2} & \text{if } 2.44 \le |k_{xy}x_{\max}|. \end{cases} \quad [34]$$

In Fig. 2 we compare the attenuation functions given by Eqs. [31] (z gradient) and [34] (transverse gradient). The number 2.44 has been obtained by numerically solving for the intersection point of the true function with the approximation.

The overall attenuation due to gradients is then simply the product

$$\bar{f} = \bar{f}_z \cdot \bar{f}_{xy}. \quad [35]$$

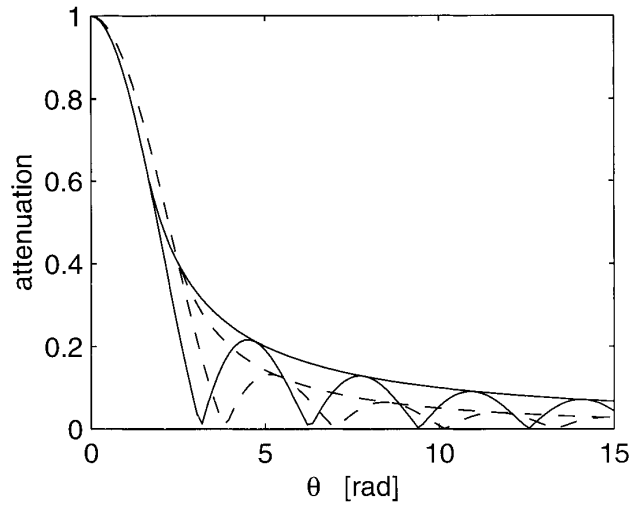

FIG. 2. Comparison between the attenuation functions due to a z gradient and a transverse gradient in a cylindrical sample as a function of $\theta = k_z z_{\max}$ and $\theta = k_x x_{\max}$, respectively. Solid lines (z gradient): $|\mathrm{sinc}(\theta)|$ + envelope function (Eq. [31]), dashed lines (transverse gradient): $|2J_1(\theta)/\theta|$ + envelope function (Eq. [34]).

By choosing a different weighting method it is possible to account for the nonuniform response throughout the active volume (*13*), gradient nonlinearity, and for non-centered gradients. Here, however, such cases are not considered since they depend on the specifics of the actual NMR instrument used.

In order to perform the calculation for all m possible pathways, a $\hat{\gamma}$*-matrix is constructed representing the pathways along its rows,

$$\hat{\gamma}^* = \begin{pmatrix} \gamma^*_{10} & \gamma^*_{11} & \cdots & \gamma^*_{1n} \\ \gamma^*_{20} & \gamma^*_{21} & \cdots & \gamma^*_{2n} \\ \cdots & \cdots & \cdots & \cdots \\ \gamma^*_{m0} & \gamma^*_{m1} & \cdots & \gamma^*_{mn} \end{pmatrix}, \quad [36]$$

where n is again the number of pulses and m the number of possible γ* pathways.

According to Eq. [28] we have

$$\begin{aligned} \hat{k} = \hat{\gamma}^* \cdot \hat{h} &= \begin{pmatrix} \gamma^*_{10} & \gamma^*_{11} & \cdots & \gamma^*_{1n} \\ \gamma^*_{20} & \gamma^*_{21} & \cdots & \gamma^*_{2n} \\ \cdots & \cdots & \cdots & \cdots \\ \gamma^*_{m0} & \gamma^*_{m1} & \cdots & \gamma^*_{mn} \end{pmatrix} \cdot \begin{pmatrix} h_{0x} & h_{1y} & h_{1z} \\ h_{1x} & h_{2y} & h_{2z} \\ \cdots & \cdots & \cdots \\ h_{nx} & h_{ny} & h_{nz} \end{pmatrix} \\ &= \begin{pmatrix} k_{1x} & k_{1y} & k_{1z} \\ k_{2x} & k_{2y} & k_{2z} \\ \cdots & \cdots & \cdots \\ k_{mx} & k_{my} & k_{mz} \end{pmatrix}, \end{aligned} \quad [37]$$

where $\hat{k}$ contains the spatial frequencies for every pathway and every gradient direction.

It remains to obtain the signal attenuations for the elements of $\hat{k}$, which is done by the procedure outlined above to calcu-

late the total attenuation for each pathway (Eqs. [31], [34], and [35]).

As in the previous section these formulas are obtained without direct reference to a particular spin system. The only requirements are that γ^* not change between the RF-pulses and that a matrix $\hat{\gamma}^*$ be constructed that reflects all possible CTPs. This might be a practical problem due to computer memory limitations in heteronuclear spin systems because the number of pathways (rows of $\hat{\gamma}^*$) can become very large.

Weighting by Diffusion

The effect of self-diffusion must always be considered when gradient sequences are constructed for the selection of CTPs, especially with large intergradient spacing and large gradient strengths. We propose a simple scheme to estimate the effects of diffusion upon a PFG sequence.

For an arbitrary gradient sequence a phenomenological diffusion term is introduced into the Bloch equations (*12, 16–18*), from which the signal attenuation

$$F(t) = \exp\left[-D \int_0^t \left(\int_0^{t'} \gamma^* \mathbf{G}(t'') dt'' \right)^2 dt' \right] \qquad [38]$$

may be derived. Diffusion is exploited in diffusion filters, e.g., for water suppression (*3, 19*). More complex situations occur if different γ^* pathways experience different effective gradients.

For the following treatment we disregard the effect of diffusion during the gradients since in spectroscopy applications they are usually short compared to the inter-gradient delays. A quick estimation should justify this statement. The Stejskal–Tanner diffusion equation (*16*) for a gradient echo is

$$F = \exp\left[-D(\gamma G \delta)^2 \left(\Delta - \frac{\delta}{3} \right) \right], \qquad [39]$$

where Δ is the delay between the starts of the two gradients, and δ is the gradient duration (rectangular shape). Neglecting diffusion during the gradients is equivalent to omitting $\frac{\delta}{3}$ in this equation. Using plausible choices for experimental parameters ($D = 2 \times 10^{-10}$ m^2 s^{-1} (diffusion coefficient of lysozyme in water at room temperature), $\delta = 2$ ms, $G = 0.5$ T m^{-1} (along the *z*-direction), and $\gamma = 2.675 \times 10^8$ rad T^{-1} s^{-1}). We obtain

$$\exp\left[D(\gamma G \delta)^2 \frac{\delta}{3} \right] = 1.0096, \qquad [40]$$

which shows that by neglecting diffusion during the gradient we make a negligibly small error. Even with very fast diffusion ($D_{H_2O} = 2.3 \times 10^{-9}$ m^2 s^{-1}) the effect is on the order of 10%. It should be emphasized that the choice of parameters is conservative, since it amounts to a case where gradient attenuation of unwanted pathways is approximately 7.5×10^{-4} (Eq. [31], assuming the active length to be 1 cm, i.e., $z_{max} = 0.5$ cm), which is usually more than necessary.

Therefore, the gradient pulses will be considered as having delta function shapes with areas of h_{ij} as defined in Eq. [27].

For a given γ^* pathway we can calculate

$$F = \exp[-D \sum_{j=x,y,z} \sum_{q=1}^{n} (\sum_{k=0}^{q-1} \gamma_k^* h_{kj})^2 \Delta_q], \qquad [41]$$

where the Δ_q are the delays between the starting points of the gradients. Because of the square in Eq. [38] the information on the gradient *direction* is lost, which reflects the fact that no direction may be attributed to isotropic diffusion.

It is now easy to generalize for a matrix $\hat{\gamma}^*$ as in Eq. [36]:

$$F_i = \exp[-D \sum_{j=x,y,z} \sum_{q=1}^{n} (\sum_{k=0}^{q-1} \gamma_{ik}^* h_{kj})^2 \Delta_q]. \qquad [42]$$

Diffusion, however, is not the only motional process affecting high-resolution NMR spectroscopy. As we pointed out recently the signal attenuation caused by convection can by far exceed the one caused by diffusion (*20, 21*). However, for its description additional information about the flow profile is needed which is seldom available. We thus defer the treatment of convection to the Appendix, where it can be seen that its inclusion requires a minor effort.

RF-Pulses and Relaxation

The approach outlined above assumes that all possible CTPs are equally probable, which ultimately leads to the construction of phase cycles which are larger than necessary.

A perfect 180° pulse is very selective in that it cleanly inverts the coherence order without mixing any pathways. A perfect 90° pulse acting on equilibrium magnetization or longitudinal one-spin order will only create ± 1 coherences. These selection rules are easily implemented in the program.

However, in real situations perfect pulses do not exist due to RF-inhomogeneity and offset dependence caused by finite power. To account for these imperfections and the attenuations of different CTPs by the RF-pulses a complete density matrix calculation for AX and AMX spin $\frac{1}{2}$ systems has been implemented. The calculation has to be performed separately for each CTP. However, we need only consider the pathways that are left over after the cancellation and attenuation by phase cycles and gradient sequences (where a threshold value determines the amount of attenuation that qualifies as cancellation). Usually it suffices to retain the strongest few hundred pathways. Alternatively, the pathway information can be used for

the input into a different simulation platform such as GAMMA (*7*), where superoperator calculus can be employed (to introduce detailed relaxation models).

It should be borne in mind that by introducing the density matrix, we digress from the principle of generality and introduce spin system specifics. Density matrix calculations are therefore an option in the program that can be enabled at the discretion of the user.

It is possible to include empirical weighting factors that can be used to account, e.g., for transverse relaxation or relative abundance on an at least phenomenological basis (which may be inaccurate but more general than an exact calculation).

IMPLEMENTATION AND EXAMPLES

We have implemented the algorithms outlined above in a MATLAB program, which we choose to call CCCP (Complete Calculation of Coherence Pathways).

All experiment dependent parameters are stored in a separate file, which is specified to the main program on the command line. An example of such an input file is displayed in Fig. 3. Detailed instructions for creating input files are given in the user manual of the program, which will be available from the authors.

The phase cycle is input in the form of vectors for each pulse (variable `ph`), and for the receiver (`phrec`) in analogy to common pulse programming languages. The base of the cycles can be chosen by `base`, `recbase`.

The `allow_paths` variable is a matrix in which restrictions and/or attenuations of the allowed CTPs can be entered. This can be done separately for every nuclear species which is indicated by the number in braces. In the example of Fig. 3 zero order coherence is chosen at the beginning of the pulse sequence, and after the first pulse only orders of $+1$, 0, -1 are permitted; -1 coherence is detected for the first nucleus (^{1}H) and zero for the second nucleus (^{13}C).

The gyromagnetic ratios for the nuclear species are input in the vector `gamma`. The `grads` array contains the gradient areas between the RF-pulses (starting before the first pulse) in units of Teslas per meter. The array can contain up to three rows to handle three-axis gradient systems. The array `sampledim` contains the sample dimensions (the active length of the receiver coil in z and the inner diameter of the NMR tube). The diffusion coefficient, `diffconst`, and the delays between the gradients, `intergrad_dels`, are used to calculate the diffusion attenuation of the pathways.

The density matrix calculations are controlled by the variables `spin_system`, `pulses`, `J`, `del`, `abundance`.

`epsilon` and `cutoff` determine the threshold to be used after the calculation of the phase cycle and the gradient attenuations, respectively.

The program first constructs the $\hat{p}$ matrix (Eq. [14]) considering the restrictions imposed by the user. The weighting factors (`allowed_paths`) are used to calculate the "empirical" weighting factors for the CTPs. The signal attenuation due to the phase cycle is calculated by means of Eqs. [15], [16], and [17], and canceled pathways are discarded (according to the specified threshold `epsilon`).

The $\hat{\gamma}^*$ matrix is constructed from $\hat{p}$ using Eq. [22] and the gradient damping is calculated using Eqs. [37], [31], [34], and [35]. Another threshold determines the pathways which are to be discarded.

Diffusion damping is calculated using Eq. [42]. Again, pathways are discarded according to the threshold.

The remaining pathways are sorted by their overall signal intensity and prepared for display and, if requested for further calculations, employ density operator calculations.

Some results of simulations with CCCP are shown in Figs. 4–9 together with the corresponding pulse sequences.

We chose three representative examples of NMR experiments to be analyzed by the program. First, a stimulated echo (STE) diffusion sequence with bipolar gradients (*22*), which should highlight the importance of the analysis of diffusion damping in the presence of pulsed field gradients. The second is a 3D homonuclear PFG 2Q-NOESY (*23*), and the third is an implementation of HSQC (*24–26*) to exemplify the application to heteronuclear spin systems.

For all simulations the eight strongest pathways are shown. The dimensions of the cylinder representing the active volume are 10 mm along z, diameter of 5 mm. For the calculation of the diffusion attenuation a diffusion coefficient of $D = 7 \times 10^{-10}$ m^2/s is assumed, which corresponds, e.g., to a medium-sized protein dissolved in water.

In the density matrix calculations some evolution delays, like the mixing time or t_1, t_2 delays, were set to a value near $1/(4J)$, so that both in-phase and anti-phase terms develop with approximately equal amplitude. A homonuclear AMX spin system with the coupling constants 16, 12, and 7 Hz was used for these calculations (with the exception of a heteronuclear AMX spin system for the HSQC example in Fig. 9, where the homonuclear and the heteronuclear coupling constants were 16 and 140 Hz, respectively, and only one proton was coupled to the carbon). No chemical shift evolution is considered since it is irrelevant here.

All simulations start out with coherence order zero (equilibrium magnetization). After the first pulse only ± 1, and zero coherence orders were allowed. The detector was assumed to cleanly select -1QC. If this criterion is left out, the effects of quadrature images and/or axial peaks can be simulated easily.

To account for imperfect pulses the flip angles were reduced to the indicated extent. No carrier offset effects were considered in the examples given.

In a first simulation of the STE diffusion sequence (Fig. 4) we have not included the information about the spin system (no density matrix calculation). All coherence orders from -3 to 3 were allowed, giving 50,421 possible pathways. The desired pathways (nos. 4 and 5), which undergo dephasing during the first two gradients and rephasing during the last two, are not the

```
function [gamma,range,allow_paths,base,ph,pulses,recbase,grads,phrec,...
      cutoff,epsilon,diffconst,intergrad_dels,sampledim,spin_system,J,...
      del,abundance]=hsqc()

ph{1}= [0]; ph{2}= [0]; ph{3}=0; ph{4}=1; ph{5}=[0 2]; ph{6}=[0 0 2 2];
ph{7}=[0 0 0 0 2 2 2 2]; ph{8}=0; ph{9}=ph{7}; ph{10}=0; ph{11}=0;
phrec= [0 2 0 2  2 0 2 0]; base=4; recbase=4;

pulses =      [[1 2 2 1 1  2 2 1 1 2  2]*pi/2*.95;...
               [1 1 2 1 2  1 2 1 2 1  2]];

allow_paths{1}=[0 0 1 1 1  1 1 1 1 1  0 0;...
                0 1 1 1 1  1 1 1 1 1  0 0;...
                1 1 1 1 1  1 1 1 1 1  0 0;...
                0 1 1 1 1  1 1 1 1 1  1 1;...
                0 0 1 1 1  1 1 1 1 1  0 0];

allow_paths{2}=[0 1 1 1 1  1 1 1 1 1  1 0;...
                1 1 1 1 1  1 1 1 1 1  1 1;...
                0 1 1 1 1  1 1 1 1 1  1 0];

gamma=[2.67522e8 0.67283e8];
gradunits=50e-2*1e-3; sampledim=1e-2;
grads =    0.1*[0 0 0 0 0 0 gamma(1)/gamma(2) 0 0 0 0 1]*gradunits;

diffconst=7e-10;
intergrad_dels=[0 0 0 0 0 0 0 0.0037 0 0 0];

spin_system='AMXinv'; abundance=[1 .01]; J=[16 140];
del=[0.0017 0 0.0017 0 0.015 0.017 0.002 0 0.0017 0 0.0017];

epsilon=1e-4;
cutoff=1e-4;
range=1:8;

return
```

FIG. 3. Sample input file to the program CCCP for the simulation of an HSQC experiment (Fig. 8).

strongest ones. The diffusion attenuation of these pathways is exploited for the determination of diffusion coefficients and to achieve diffusion separation in DOSY experiments (*20, 27–29*). The spoiler gradients during T and T_e are used to defocus everything but zero quantum coherence. It is clear from the graph, however, that pathways will be retained which are affected only by one lobe of the bipolar gradient (nos. 1 and 2). Diffusion damping is weaker for those, as can be seen in the table in Fig. 4. Even triple quantum terms may occur (pathway nos. 3, 6–8). These pathways are caused by the imperfections of the 180° pulses and would lead to erroneous results in the determination of diffusion coefficients.

Given such an analysis we would be tempted to implement a longer phase cycle to remove the unwanted pathways. How-

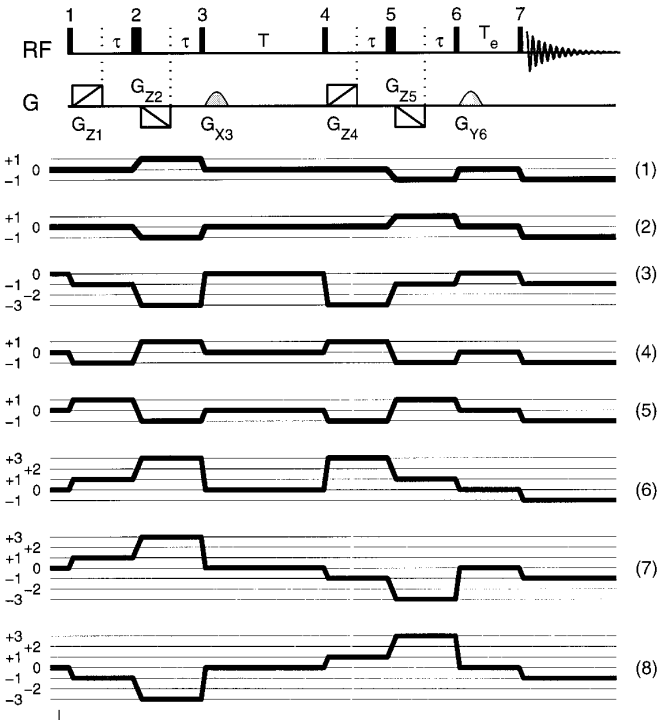

No.	total	ψ	norm	pc	grad	diff
1	0.5971	45	1.0000	0.7071	1.0000	0.8445
2	0.5971	315	1.0000	0.7071	1.0000	0.8445
3	0.5150	0	0.8624	1.0000	1.0000	0.5150
4	0.5150	0	0.8624	1.0000	1.0000	0.5150
5	0.5150	0	0.8624	1.0000	1.0000	0.5150
6	0.5150	0	0.8624	1.0000	1.0000	0.5150
7	0.4898	0	0.8202	1.0000	1.0000	0.4898
8	0.4898	0	0.8202	1.0000	1.0000	0.4898

FIG. 4. CCCP simulation of a stimulated gradient echo diffusion sequence employing bipolar gradient pulses ramped to give a pseudo-t_1 dimension (rectangles with a diagonal) and a longitudinal eddy current delay T_e. Narrow and wide bars represent 90 and 180 degree pulses. All gradients are labeled according to the direction along which they are applied. G_{X3} and G_{Y6} are spoiler gradients used to defocus transverse magnetization during T and T_e. Phase cycle: $\phi(1) = x, x, y, y, -x, -x, -y, -y$; $\phi(2) = y, -x, -x, -y, -y, x, x, y$; $\phi(3) = \phi(7) = x$; $\phi(4) = -x, -x, -y, -y$; $\phi(5) = -y, -y, x, x$; $\phi(6) = -x$; ϕ(receiver) $= 2(x, -x), 2(-x, x)$. The gradient strengths were 0.25 T/m for each of the bipolar gradient lobes (gradients G_{Z1}, $-G_{Z2}$, G_{Z4}, $-G_{Z5}$), 0.025 T/m for each of the spoiler gradients (G_{X3}, G_{Y3}), duration 1 ms. The inter-gradient delays were 2, 2, 50, 2, and 2 ms. No density matrix calculation was made. The following signal attenuations are given in the table at the bottom: total—total signal attenuation; norm—normalized to the strongest pathway, pc—attenuation due to phase cycle; grad—attenuation due to the gradients, diff—attenuation due to diffusion; ψ—phases of the pathways.

ever, we have not yet considered that the RF-pulses cause an additional attenuation of the CTPs. In a second simulation run we included a density matrix calculation for an AMX spin system using pulses with flip angles which were 5% short (to accommodate imperfect pulses). The results are displayed in Fig. 5. In this analysis the desired pathways end up in the first two positions. The strongest remaining undesired pathways have now an intensity of up to 1% as compared to the desired pathways (if compared to the sum of the two desired pathways, they have only up to 0.5% of intensity). These pathways can be further attenuated by increasing the spoiler gradients during T and T_e. The success of this particular pulse sequence and phase cycle has been proven by experiment (*20, 29, 30*).

In Fig. 6 the results of a simulation of a 3D homonuclear PFG 2Q-NOESY (*23*) are shown (352,947 pathways have to be considered, again with a maximum coherence order of 3). The delays and gradient strengths were set such as to reflect those of the original publication (*23*) (with the exception of the mixing time, and t_1, t_2, where intermediate values were taken as described above). The pulses were set 3% short in this case. Pulses 1–3 perform a NOESY step with t_1 labeling (G_1 spoils transverse magnetization during the NOESY mixing time), and pulses 3–5 excite double quantum coherence, which evolves during t_2 and is subsequently transformed to single quantum coherence for detection. Due to the imperfections of pulse 4 some undesired pathways (nos. 5–8) are retained with a fairly high intensity (up to 8.9% of the strongest pathways). These may cause phase errors in the spectra. In an attempt to atten-

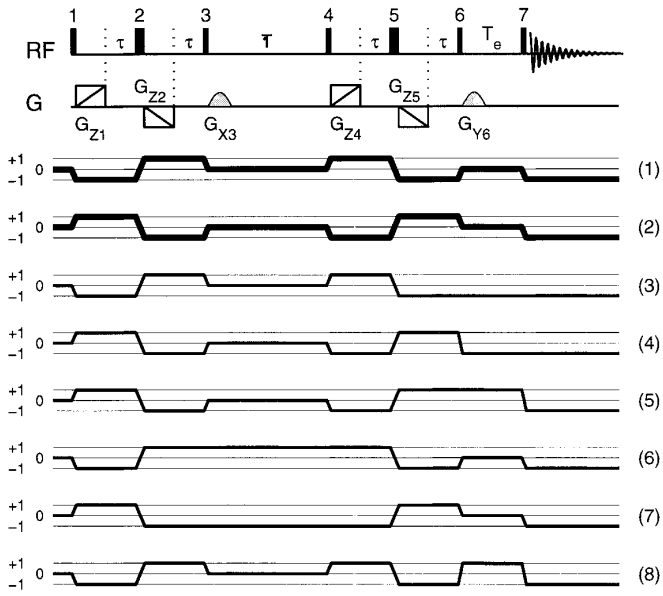

No.	total	ψ	norm	pc	grad	diff	pulse
1	0.2349	180	1.0000	1.0000	1.0000	0.5150	-0.4562
2	0.2349	180	1.0000	1.0000	1.0000	0.5150	-0.4562
3	0.0024	180	0.0104	1.0000	0.0233	0.5101	0.2053
4	0.0022	0	0.0096	1.0000	0.0233	0.5101	-0.1888
5	0.0021	0	0.0089	1.0000	0.0233	0.5101	-0.1754
6	0.0021	225	0.0087	0.7071	0.0233	0.5093	0.2440
7	0.0021	135	0.0087	0.7071	0.0233	0.5093	0.2440
8	0.0019	180	0.0082	1.0000	0.0233	0.5101	0.1613

FIG. 5. CCCP simulation of a stimulated gradient echo diffusion sequence with bipolar gradient pulses and a longitudinal eddy current delay. The sequence and parameters are the same as those in Fig. 4 but an AMX density matrix calculation was employed with all pulses 5% short. The evolution delays were 2, 2, 15, 2, 2, and 15 ms. The column "pulse" in the table contains the attenuation factors due to the density matrix calculations.

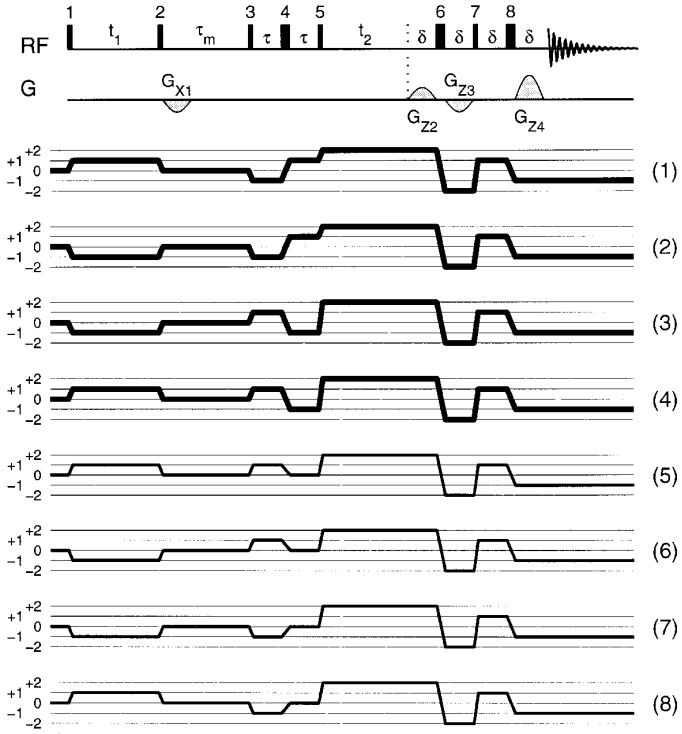

No.	total	ψ	norm	pc	grad	diff	pulse
1	0.0217	180	1.0000	1.0000	1.0000	0.9864	-0.0220
2	0.0215	180	0.9929	1.0000	1.0000	0.9864	-0.0218
3	0.0214	180	0.9845	1.0000	1.0000	0.9864	-0.0217
4	0.0212	180	0.9785	1.0000	1.0000	0.9864	-0.0215
5	0.0019	0	0.0887	1.0000	1.0000	0.9864	0.0020
6	0.0019	0	0.0883	1.0000	1.0000	0.9864	0.0019
7	0.0018	180	0.0818	1.0000	1.0000	0.9864	-0.0018
8	0.0018	180	0.0815	1.0000	1.0000	0.9864	-0.0018

FIG. 6. CCCP simulation of a 3D homonuclear PFG 2Q-NOESY (*23*). The phase cycle is $\phi(1) = 4x, 4(-x)$; $\phi(8) = x, -y, -x, y$; ϕ(receiver) $= 2(x, -x), 2(-x, x)$; all other phases remain constant at x. The parameters were taken mainly from (*23*), i.e., $G_{X1} = 0.05$ T/m, $G_{Z2} = -G_{Z3} = 0.05$ T/m, $G_{Z4} = 0.2$ T/m. The gradient duration δ is 1.25 ms. Only the delays between G_{Z2}, G_{Z3}, and G_{Z4} are important for the diffusion damping (since G_{X1} is orthogonal to them), which were 1.35, and 2.7 ms, respectively. For the density matrix calculations the pulses were set 3% short, and the following inter-RF-pulse delays were used: 15, 15, 15, 15, 7.5, 1.35, 1.35, and 1.35 ms.

uate then further we introduce two new gradients, G_5 and G_6, orthogonal to the other ones, into the pulse sequence. The results of this new simulation are displayed in Fig. 7, where it is seen that we have effectively suppressed the troublesome pathways. However, new, undesired pathways appear in the positions 5–8. These involve triple quantum coherence between the pulses 3 and 5, which is refocused by pulse 4. Therefore these pathways do not give rise to phase errors. However, since their phase is opposite to the desired pathways they may cause signal attenuation.

The desired pathways 1–4 have coherence orders of ± 1 during t_1 and can thus be used for phase sensitive detection using TPPI (*31, 32*) or States–TPPI (*33, 34*). Phase sensitive detection in t_2 can only be performed by changing the polarity of G_2 and G_3 in consecutive scans as mentioned in (*23*). The result of such a scan is displayed in Fig. 8. The coherence orders during t_2 are opposite.

A word is in order about the differences in the attenuations of the first four pathways (the desired pathways) in Figs. 6–8. They can be explained by the fact that the pulses are 3% short, which causes them to excite positive and negative coherence orders with different intensities. These differences are usually not observed since the flip angle error due to RF-inhomogeneity is averaged over the entire sample volume.

The last example shows the pathway selection for HSQC (Fig. 9). Here, the allowed coherence orders range from -2 to 2 for protons and from -1 to $+1$ for carbons (151,875 pathways). The parameters for this simulation are shown in Fig. 3. It is important to note that the strongest pathways all involve transfers in the carbon coherence orders, meaning that proton

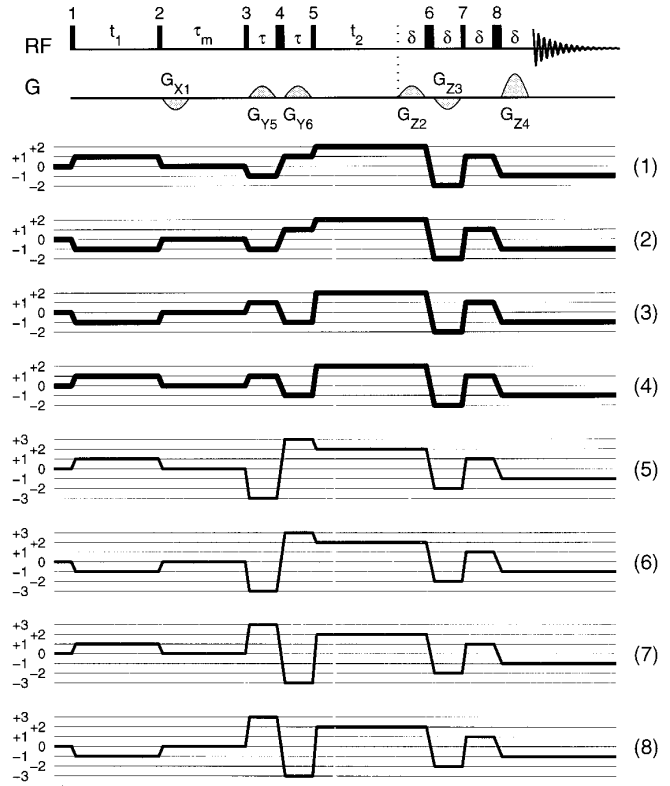

No.	total	ψ	norm	pc	grad	diff	pulse
1	0.0216	180	1.0000	1.0000	1.0000	0.9835	-0.0220
2	0.0215	180	0.9929	1.0000	1.0000	0.9835	-0.0218
3	0.0213	180	0.9845	1.0000	1.0000	0.9835	-0.0217
4	0.0212	180	0.9785	1.0000	1.0000	0.9835	-0.0215
5	0.0014	0	0.0654	1.0000	1.0000	0.9606	0.0015
6	0.0014	0	0.0654	1.0000	1.0000	0.9606	0.0015
7	0.0012	0	0.0542	1.0000	1.0000	0.9606	0.0012
8	0.0012	0	0.0542	1.0000	1.0000	0.9606	0.0012

FIG. 7. CCCP simulation of a 3D homonuclear PFG 2Q-NOESY (*23*). The parameters are the same as those in Fig. 6 but two new gradients, $G_{Y5} = G_{Y6} = 0.05$ T/m, were inserted (with a spacing of 15 ms).

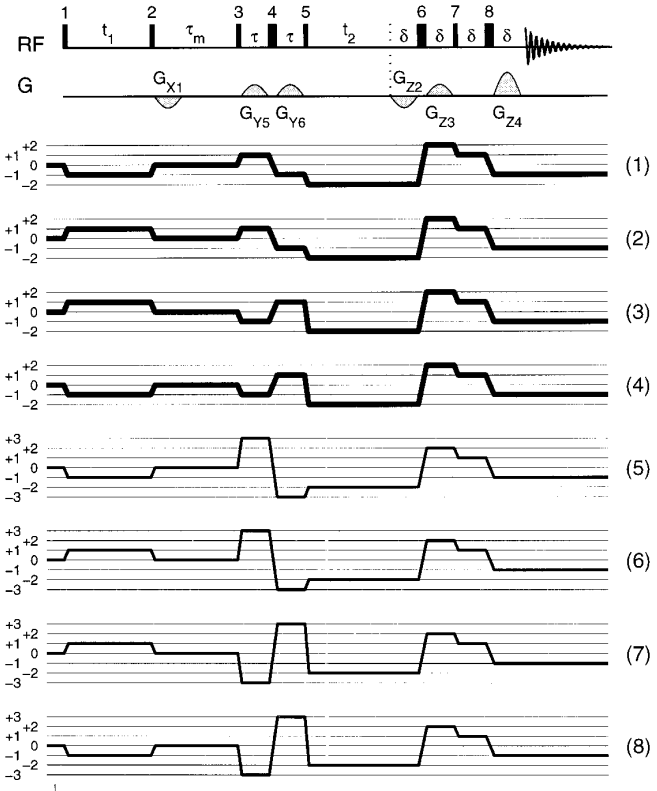

No.	total	ψ	norm	pc	grad	diff	pulse
1	0.0238	180	1.0000	1.0000	1.0000	0.9835	-0.0242
2	0.0236	180	0.9930	1.0000	1.0000	0.9835	-0.0240
3	0.0235	180	0.9863	1.0000	1.0000	0.9835	-0.0239
4	0.0233	180	0.9805	1.0000	1.0000	0.9835	-0.0237
5	0.0016	0	0.0670	1.0000	1.0000	0.9606	0.0017
6	0.0016	0	0.0670	1.0000	1.0000	0.9606	0.0017
7	0.0013	0	0.0555	1.0000	1.0000	0.9606	0.0014
8	0.0013	0	0.0555	1.0000	1.0000	0.9606	0.0014

FIG. 8. CCCP simulation of a 3D homonuclear PFG 2Q-NOESY (*23*). The parameters are the same as those in Fig. 7 but the polarity of the gradients G_{Z2} and G_{Z3} is flipped, leading to echo type coherence selection during t_2 (as opposed to anti-echo type in Fig. 7).

signals not attached to ^{13}C are well attenuated. The density matrix calculation was performed using an AMX spin system consisting of two ^{1}H and one ^{13}C nuclei. An abundance factor of 1% was used to account for the rare natural abundance of ^{13}C. Only one proton (the one coupled to the carbon) was detected. Ideal decoupling was assumed.

CONCLUSION

The formalism presented here is a valuable tool for the design of optimized phase cycles and gradient sequences in pulse sequences applicable to different kinds of nuclei and spin systems (in NMR and EPR likewise). The method is both general and time efficient. It involves the construction of all possible CTPs, the calculation of their attenuation by phase cycling, gradient sequences, diffusion, and RF-pulses. The effects of convection can be included easily as is shown in the Appendix, which can be useful for the design of gradient enhanced experiments with convection compensation (*20, 21*). The treatment of diffusion is very important particularly for the simulation and optimization of NMR diffusion pulse sequences

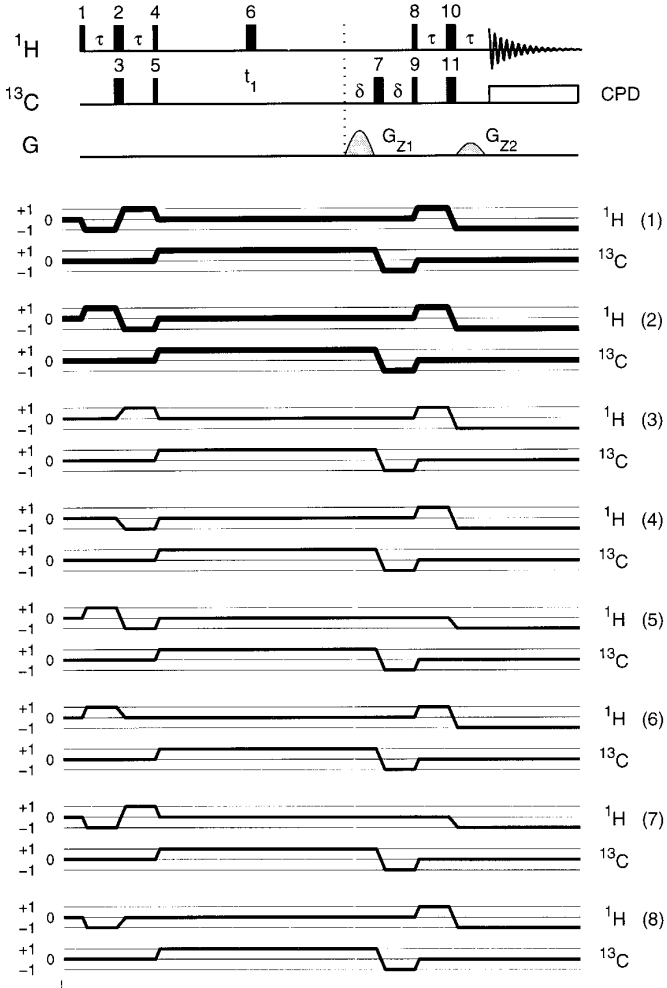

No.	total	ψ	norm	pc	grad	diff	pulse
1	0.4491	90	1.0000	1.0000	1.0000	0.9995	0.4493
2	0.4489	90	0.9995	1.0000	1.0000	0.9995	-0.4491
3	0.0039	270	0.0087	1.0000	1.0000	0.9995	-0.0039
4	0.0039	270	0.0087	1.0000	1.0000	0.9995	0.0039
5	0.0039	270	0.0086	1.0000	1.0000	0.9995	0.0039
6	0.0038	0	0.0085	1.0000	1.0000	0.9995	0.0038
7	0.0038	270	0.0084	1.0000	1.0000	0.9995	-0.0038
8	0.0038	180	0.0084	1.0000	1.0000	0.9995	-0.0038

FIG. 9. CCCP simulation of a HSQC experiment including a density matrix calculation for an AMX system. The phase cycle is $\phi(4) = y$; $\phi(5) = x, -x$; $\phi(6) = x, x, -x, -x$; $\phi(7) = \phi(9) = 4x, 4(-x)$; ϕ(receiver) $= 2(x, -x), 2(-x, x)$; all other phases are constant at x. For the diffusion weighting only the delay $\delta + \tau$, which was set to 3.7 ms, is relevant. The pulses were set 5% short, and the evolution delays 1.7, 1.7, 15, 17, 2, 1.7, and 1.7 ms were used. The gradient strengths were 0.199, and 0.05 T/m at 1 ms duration. For the eight strongest pathways the partial coherence orders of protons and carbons are displayed separately.

and applications of diffusion separated NMR (*20, 27–29*) as well as diffusion filters (*3, 19*).

The pathways can be visually inspected in a graphical display and empirical knowledge may be used to filter out possibly redundant and irrelevant information. If exact results on spin dynamics are required a detailed simulation may be appended using the results of our general calculations, which, however, implies giving up generality. This algorithm has been implemented in a MATLAB program (CCCP), which is available from the authors upon request.

The approach is practically limited by the amount of computer memory available (the number of possible CTPs rises to the power of the number of pulses involved). When the memory limit is reached, the problem can still be solved by analyzing parts of the pulse sequences separately, since the coherence orders before the pulses and at the end can be specified by the user at will.

We believe that the CCCP approach fills a gap in the field of NMR simulations. As we could show, the examination of the relative attenuation of different CTPs caused by different filtering techniques is of valuable help for the design of phase cycles and gradient sequences. Using our method we optimized an experiment published in Ref. (*23*) and propose here an improvement of the CTP selection method for a 3D homonuclear PFG 2Q-NOESY experiment, which may be useful in practice.

APPENDIX

We have shown recently that the effect of convection on the signal attenuation in gradient enhanced spectra can be very strong (*20, 21*). Here, we present a simple mathematical description thereof and a method for the incorporation into the formalism presented in the main part of the article.

A signal following a particular γ^* pathway acquires the location $\mathbf{r}$ dependent phase

$$\psi(\mathbf{r}) = \int_0^t \gamma^*(t')\mathbf{G}(t')\cdot\mathbf{r}(t')dt'. \qquad [43]$$

Using the expansion $\mathbf{r} = \mathbf{r}_0 + \mathbf{v}t + \frac{1}{2}\mathbf{a}t^2 + \cdots$ we can write

$$\psi = \mathbf{r}_0 \underbrace{\int_0^t \gamma^*(t')\mathbf{G}(t')dt'}_{\text{0th moment}} + \mathbf{v}\underbrace{\int_0^t \gamma^*(t')\mathbf{G}(t')t'dt'}_{\text{1st moment}}$$

$$+ \frac{1}{2}\mathbf{a}\underbrace{\int_0^t \gamma^*(t')\mathbf{G}(t')t'^2dt'}_{\text{2nd moment}} + \cdots. \qquad [44]$$

We have treated the influence of the zeroth moment in the main text by calculating the attenuation of the different CTPs by the gradient sequence. We have not yet, however, considered higher moments. All higher moments introduce additional constant phase shifts if $\mathbf{v}$, $\mathbf{a}$, etc. are kept the same for the duration of the experiment, and uniform over the sample volume. For simplicity we shall be concerned only with $\mathbf{v}$ being constant and non-zero (i.e., no flow acceleration). In this case only a phase factor proportional to the velocity is introduced. When a velocity distribution $f(\mathbf{v})$ exists in the sample, the ensemble average results in the signal attenuation

$$F = \int f(\mathbf{v})\exp(-i\psi(\mathbf{v}))d\mathbf{v}, \qquad [45]$$

where the integral is taken over the ranges of the velocities v_x, v_y, v_z, and $\psi(\mathbf{v}) = \mathbf{v}\int_0^t \gamma^*(t')\mathbf{G}(t')t'dt'$.

Using the same simplifying assumptions as those used with the diffusion weighting (neglect of motion during the gradient pulses) we calculate $\psi(\mathbf{v})$ as

$$\psi(\mathbf{v}) = \mathbf{v}\cdot\sum_{i=1}^{n}\gamma_i^*(h_{ix}, h_{iy}, h_{iz})^T t_i, \qquad [46]$$

where h_{ij} is defined in Eq. [27], $\mathbf{v} = (v_x, v_y, v_z)$, and t_i is the time of the ith RF-pulse.

In order to calculate the signal attenuation we have to make an assumption about the velocity distribution. A simple case is a uniform distribution between $-v_{\max}$ and $v_{\max}$ (in the z-direction) and no motion in the x- and y-directions:

$$f(\mathbf{v}) = \delta(v_x)\cdot\delta(v_y)\cdot\begin{cases}\dfrac{1}{2v_{\max}} & \text{if } |v_z| \le v_{\max}\\ 0 & \text{if } |v_z| > v_{\max}.\end{cases} \qquad [47]$$

The signal attenuation is then calculated from Eq. [45] to

$$F = \operatorname{sinc}(\psi(v_{\max})), \qquad [48]$$

which can be done separately for every γ^* pathway by use of Eq. [46].

ACKNOWLEDGMENTS

This work was supported by the Austrian Science Foundation, "Fonds zur Förderung der Wissenschaftlichen Forschung (FWF)," Project P 10633-ÖCH. We are grateful to one of the reviewers for helping us to fix a flaw in connection with the calculation of the gradient attenuation in cylindrical samples, and also otherwise very constructive comments.

REFERENCES

1. A. D. Bain, *J. Magn. Reson.* **56,** 418 (1984).
2. G. Bodenhausen, H. Kogler, and R. R. Ernst, *J. Magn. Reson.* **58,** 370 (1984).
3. J. Keeler, R. T. Clowes, A. L. Davis, and E. D. Laue, *in* "Methods in Enzymology," Vol. 239, p. 145, Academic Press, San Diego (1994).
4. C. Gemperle, G. Aebli, A. Schweiger, and R. R. Ernst, *J. Magn. Reson.* **88,** 241 (1990).
5. J.-M. Fauth, A. Schweiger, L. Braunschweiler, and R. R. Ernst, *J. Magn. Reson.* **66,** 74 (1986).
6. L. Mitschang, H. Ponstingl, D. Grindrod, and H. Oschkinat, *J. Chem. Phys.* **102,** 3089 (1995).
7. S. A. Smith, T. O. Levante, B. H. Meier, and R. R. Ernst, *J. Magn. Reson. A* **106,** 75 (1994).
8. P. Güntert, N. Schaefer, G. Otting, and K. Wüthrich, *J. Magn. Reson. A* **101,** 103 (1993).
9. P. B. Kingsley, *J. Magn. Reson. A* **107,** 14 (1994).
10. R. R. Ernst, G. Bodenhausen, and A. Wokaun, "Principles of Nuclear Magnetic Resonance in One and Two Dimensions," Clarendon Press, Oxford (1987).
11. M. E. Rose, "Elementary Theory of Angular Momentum," Wiley, New York (1966).
12. P. T. Callaghan, "Principles of Nuclear Magnetic Resonance Microscopy," Oxford Univ. Press, London (1993).
13. P. B. Kingsley, *J. Magn. Reson. B* **109,** 243 (1995).
14. I. S. Gradshteyn and I. M. Ryzhnik, "Table of Integrals, Series, and Products," Academic Press, San Diego (1994).
15. G. A. Korn and T. M. Korn, "Mathematical Handbook for Scientists and Engineers," McGraw–Hill, New York (1968).
16. E. O. Stejskal and J. E. Tanner, *J. Chem. Phys.* **42,** 288 (1965).
17. E. O. Stejskal, *J. Chem. Phys.* **43,** 3597 (1965).
18. H. C. Torrey, *Phys. Rev.* **104,** 563 (1956).
19. G. Wider, R. Riek, and K. Wüthrich, *J. Am. Chem. Soc.* **118,** 11629 (1996).
20. A. Jerschow and N. Müller, *J. Magn. Reson.* **125,** 372 (1997).
21. A. Jerschow and N. Müller, *J. Magn. Reson.* **132,** 13 (1998).
22. D. Wu, A. Chen, and C. S. Johnson, Jr., *J. Magn. Reson. A* **115,** 260 (1995).
23. C. Dalvit, *J. Magn. Reson. B* **112,** 186 (1996).
24. L. E. Kay, P. Keifer, and T. Saarinen, *J. Am. Chem. Soc.* **114,** 10663 (1992).
25. A. G. Palmer III, J. Cavanagh, P. E. Wright, and M. Rance, *J. Magn. Reson.* **93,** 151 (1991).
26. G. Kontaxis, J. Stonehouse, E. D. Laue, and J. Keeler, *J. Magn. Reson. A* **111,** 70 (1994).
27. K. F. Morris, P. Stilbs, and C. S. Johnson, Jr., *Anal. Chem.* **66,** 211 (1995).
28. H. Barjat, G. A. Morris, S. Smart, A. G. Swanson, and S. C. R. Williams, *J. Magn. Reson. B* **108,** 170 (1995).
29. A. Jerschow and N. Müller, *J. Magn. Reson. A* **123,** 222 (1996).
30. E. J. Fordham, S. J. Gibbs, and L. D. Hall, *Magn. Reson. Imag.* **12,** 279 (1994).
31. G. Drobny, A. Pines, S. Sinton, D. P. Weitenkamp, and D. Wemmer, *Faraday Symp. Chem. Soc.* **13,** 49 (1979).
32. D. Marion and K. Wüthrich, *Biochem. Biophys. Res. Commun.* **113,** 967 (1983).
33. P. Bachmann, W. P. Aue, L. Müller, and R. R. Ernst, *J. Magn. Reson.* **28,** 29 (1977).
34. D. J. States, R. A. Haberkorn, and D. J. Ruben, *J. Magn. Reson.* **48,** 286 (1982).